

Search for Ultra High-Energy Neutrinos with AMANDA-II

IceCube Collaboration: M. Ackermann³³, J. Adams¹¹, J. Ahrens²², K. Andeen²¹, J. Auffenberg³², X. Bai²⁴, B. Baret⁹, S. W. Barwick¹⁶, R. Bay⁵, K. Beattie⁷, T. Becka²², J. K. Becker¹³, K.-H. Becker³², M. Beimforde⁶, P. Berghaus⁸, D. Berley¹², E. Bernardini³³, D. Bertrand⁸, D. Z. Besson¹⁸, E. Blaufuss¹², D. J. Boersma²¹, C. Boehm²⁷, J. Bolmont³³, S. Böser³³, O. Botner³⁰, A. Bouchta³⁰, J. Braun²¹, T. Burgess²⁷, T. Castermans²³, D. Chirkin⁷, B. Christy¹², J. Clem²⁴, D. F. Cowen^{29,28}, M. V. D'Agostino⁵, A. Davour³⁰, C. T. Day⁷, C. De Clercq⁹, L. Demirörs²⁴, F. Descamps¹⁴, P. Desiati²¹, G. de Vries-Uiterweerd³¹, T. DeYoung²⁹, J. C. Diaz-Velez²¹, J. Dreyer¹³, J. P. Dumm²¹, M. R. Duvoort³¹, W. R. Edwards⁷, R. Ehrlich¹², J. Eisch²¹, R. W. Ellsworth¹², P. A. Evenson²⁴, O. Fadiran³, A. R. Fazely⁴, K. Filimonov⁵, C. Finley²¹, M. M. Foerster²⁹, B. D. Fox²⁹, A. Franckowiak³², R. Franke³³, T. K. Gaisser²⁴, J. Gallagher²⁰, R. Ganugapati²¹, H. Geenen³², L. Gerhardt^{16,*}, A. Goldschmidt⁷, J. A. Goodman¹², R. Gozzini²², T. Griesel²², A. Groß¹⁵, S. Grullon²¹, R. M. Gunasingha⁴, M. Gurtner³², C. Ha²⁹, A. Hallgren³⁰, F. Halzen²¹, K. Han¹¹, K. Hanson²¹, D. Hardtke⁵, R. Hardtke²⁶, Y. Hasegawa¹⁰, T. Hauschildt²⁴, J. Heise³¹, K. Helbing³², M. Hellwig²², P. Herquet²³, G. C. Hill²¹, J. Hodges²¹, K. D. Hoffman¹², B. Hommez¹⁴, K. Hoshina²¹, D. Hubert⁹, B. Hughey²¹, J.-P. Hülß¹, P. O. Hulth²⁷, K. Hultqvist²⁷, S. Hundertmark²⁷, M. Inaba¹⁰, A. Ishihara¹⁰, J. Jacobsen²¹, G. S. Japaridze³, H. Johansson²⁷, J. M. Joseph⁷, K.-H. Kampert³², A. Kappes^{21,a}, T. Karg³², A. Karle²¹, H. Kawai¹⁰, J. L. Kelley²¹, J. Kiryluk⁷, F. Kislat⁶, N. Kitamura²¹, S. R. Klein⁷, S. Klepser³³, G. Kohnen²³, H. Kolanoski⁶, L. Köpke²², M. Kowalski⁶, T. Kowarik²², M. Krasberg²¹, K. Kuehn¹⁶, T. Kuwabara²⁴, M. Labare⁸, K. Laihem¹, H. Landsman²¹, R. Lauer³³, H. Leich³³, D. Leier¹³, I. Liubarsky¹⁹, J. Lundberg³⁰, J. Lünemann¹³, J. Madsen²⁶, R. Maruyama²¹, K. Mase¹⁰, H. S. Matis⁷, T. McCauley⁷, C. P. McParland⁷, K. Meagher¹², A. Meli¹³, T. Messarius¹³, P. Mészáros^{29,28}, H. Miyamoto¹⁰, T. Montaruli^{21,b}, A. Morey⁵, R. Morse²¹, S. M. Movit²⁸, K. München¹³, R. Nahnauer³³, J. W. Nam¹⁶, P. Nießen²⁴, D. R. Nygren⁷, A. Olivas¹², M. Ono¹⁰, S. Patton⁷, C. Pérez de los Heros³⁰, A. Piegsa²², D. Pieloth³³, A. C. Pohl^{30,c}, R. Porrata⁵, J. Pretz¹², P. B. Price⁵, G. T. Przybylski⁷, K. Rawlins², S. Razzaque^{29,28}, P. Redl¹², E. Resconi¹⁵, W. Rhode¹³, M. Ribordy¹⁷, A. Rizzo⁹, S. Robbins³², W. J. Robbins²⁹, P. Roth¹², F. Rothmaier²², C. Rott²⁹, C. Roucelle⁷, D. Rutledge²⁹, D. Ryckbosch¹⁴, H.-G. Sander²², S. Sarkar²⁵, K. Satalecka³³, S. Schlenstedt³³, T. Schmidt¹², D. Schneider²¹, O. Schultz¹⁵, D. Seckel²⁴, B. Semburg³², S. H. Seo²⁹, Y. Sestayo¹⁵, S. Seunarine¹¹, A. Silvestri¹⁶, A. J. Smith¹², C. Song²¹, G. M. Spiczak²⁶, C. Spiering³³, M. Stamatikos^{21,d}, T. Stanev²⁴, T. Stezelberger⁷, R. G. Stokstad⁷, M. C. Stoufer⁷, S. Stoyanov²⁴, E. A. Strahler²¹, T. Straszheim¹², K.-H. Sulanke³³, G. W. Sullivan¹², T. J. Sumner¹⁹, Q. Swillens⁸, I. Taboada⁵,

O. Tarasova³³, A. Tepe³², L. Thollander²⁷, S. Tilav²⁴, M. Tluczykont³³, P. A. Toale²⁹,
D. Tosi³³, D. Turčan¹², N. van Eijndhoven³¹, J. Vandenbroucke⁵, A. Van Overloop¹⁴,
V. Viscomi²⁹, C. Vogt¹, B. Voigt³³, W. Wagner²⁹, C. Walck²⁷, H. Waldmann³³,
T. Waldenmaier²⁴, M. Walter³³, Y.-R. Wang²¹, C. Wendt²¹, C. H. Wiebusch¹,
C. Wiedemann²⁷, G. Wikström²⁷, D. R. Williams²⁹, R. Wischnewski³³, H. Wissing¹,
K. Woschnagg⁵, X. W. Xu⁴, G. Yodh¹⁶, S. Yoshida¹⁰, J. D. Zornoza^{21,e}

*Corresponding author: gerhardt@hep.ps.uci.edu

¹III Physikalisches Institut, RWTH Aachen University, D-52056 Aachen, Germany

²Dept. of Physics and Astronomy, University of Alaska Anchorage, 3211 Providence Dr., Anchorage, AK 99508, USA

³CTSPS, Clark-Atlanta University, Atlanta, GA 30314, USA

⁴Dept. of Physics, Southern University, Baton Rouge, LA 70813, USA

⁵Dept. of Physics, University of California, Berkeley, CA 94720, USA

⁶Institut für Physik, Humboldt-Universität zu Berlin, D-12489 Berlin, Germany

⁷Lawrence Berkeley National Laboratory, Berkeley, CA 94720, USA

⁸Université Libre de Bruxelles, Science Faculty CP230, B-1050 Brussels, Belgium

⁹Vrije Universiteit Brussel, Dienst ELEM, B-1050 Brussels, Belgium

¹⁰Dept. of Physics, Chiba University, Chiba 263-8522 Japan

¹¹Dept. of Physics and Astronomy, University of Canterbury, Private Bag 4800, Christchurch, New Zealand

¹²Dept. of Physics, University of Maryland, College Park, MD 20742, USA

¹³Dept. of Physics, Universität Dortmund, D-44221 Dortmund, Germany

¹⁴Dept. of Subatomic and Radiation Physics, University of Gent, B-9000 Gent, Belgium

¹⁵Max-Planck-Institut für Kernphysik, D-69177 Heidelberg, Germany

¹⁶Dept. of Physics and Astronomy, University of California, Irvine, CA 92697, USA

¹⁷Laboratory for High Energy Physics, École Polytechnique Fédérale, CH-1015 Lausanne, Switzerland

¹⁸Dept. of Physics and Astronomy, University of Kansas, Lawrence, KS 66045, USA

¹⁹Blackett Laboratory, Imperial College, London SW7 2BW, UK

²⁰Dept. of Astronomy, University of Wisconsin, Madison, WI 53706, USA

²¹Dept. of Physics, University of Wisconsin, Madison, WI 53706, USA

²²Institute of Physics, University of Mainz, Staudinger Weg 7, D-55099 Mainz, Germany

²³University of Mons-Hainaut, 7000 Mons, Belgium

²⁴Bartol Research Institute and Department of Physics and Astronomy, University of Delaware, Newark, DE 19716, USA

²⁵Dept. of Physics, University of Oxford, 1 Keble Road, Oxford OX1 3NP, UK

²⁶Dept. of Physics, University of Wisconsin, River Falls, WI 54022, USA

²⁷Dept. of Physics, Stockholm University, SE-10691 Stockholm, Sweden

²⁸Dept. of Astronomy and Astrophysics, Pennsylvania State University, University Park, PA 16802, USA

ABSTRACT

A search for diffuse neutrinos with energies in excess of 10^5 GeV is conducted with AMANDA-II data recorded between 2000 and 2002. Above 10^7 GeV, the Earth is essentially opaque to neutrinos. This fact, combined with the limited overburden of the AMANDA-II detector (roughly 1.5 km), concentrates these ultra high-energy neutrinos at the horizon. The primary background for this analysis is bundles of downgoing, high-energy muons from the interaction of cosmic rays in the atmosphere. No statistically significant excess above the expected background is seen in the data, and an upper limit is set on the diffuse all-flavor neutrino flux of $E^2 \Phi_{90\%CL} < 2.7 \times 10^{-7} \text{ GeV cm}^{-2} \text{ s}^{-1} \text{ sr}^{-1}$ valid over the energy range of 2×10^5 GeV to 10^9 GeV. A number of models which predict neutrino fluxes from active galactic nuclei are excluded at the 90% confidence level.

Subject headings: neutrino telescope, AMANDA, IceCube, diffuse sources, ultra high-energy

1. Introduction

AMANDA-II (Antarctic Muon and Neutrino Detector Array), a neutrino telescope at the geographical South Pole designed to detect Cherenkov light from secondary particles produced in collisions between neutrinos and Antarctic ice, has placed limits on the flux from point-like and diffuse sources of astrophysical neutrinos (Achterberg et al. 2007;

²⁹Dept. of Physics, Pennsylvania State University, University Park, PA 16802, USA

³⁰Division of High Energy Physics, Uppsala University, S-75121 Uppsala, Sweden

³¹Dept. of Physics and Astronomy, Utrecht University/SRON, NL-3584 CC Utrecht, The Netherlands

³²Dept. of Physics, University of Wuppertal, D-42119 Wuppertal, Germany

³³DESY, D-15735 Zeuthen, Germany

^aon leave of absence from Universität Erlangen-Nürnberg, Physikalisches Institut, D-91058, Erlangen, Germany

^bon leave of absence from Università di Bari, Dipartimento di Fisica, I-70126, Bari, Italy

^caffiliated with School of Pure and Applied Natural Sciences, Kalmar University, S-39182 Kalmar, Sweden

^dNASA Goddard Space Flight Center, Greenbelt, MD 20771, USA

^eaffiliated with IFIC (CSIC-Universitat de València), A. C. 22085, 46071 Valencia, Spain

Ackermann et al. 2004, 2005; Ahrens et al. 2003a,b). This work describes a search for neutrinos with energies above 10^5 GeV, which we define as ultra high-energy (UHE) neutrinos. These neutrinos are of interest because they could be associated with the potential acceleration of hadrons by active galactic nuclei (Mannheim 1995; Mannheim et al. 2000; Halzen & Zas 1997; Protheroe 1996; Stecker et al. 1992); they could potentially be produced by exotic phenomena such as the decay of topological defects (Sigl et al. 1998) or possibly associated with the Z-burst mechanism (Yoshida et al. 1998); and they are guaranteed by-products of the interactions of high-energy cosmic rays with the cosmic microwave background (Engel et al. 2001).

This analysis is sensitive to all three flavors of neutrinos. Leptons and cascades from UHE electron, muon and tau neutrinos create bright, energetic events (Fig. 1) which can be identified by AMANDA-II as far as 450 m from the center of the array (Fig. 2). The sensitivity of this analysis starts at energies roughly coincident with the highest energy threshold of other diffuse analyses conducted with AMANDA-II (Achterberg et al. 2007; Ackermann et al. 2004).

At UHE energies, the interaction length of neutrinos in rock is shorter than the diameter of the Earth (Gandhi et al. 1998), so neutrinos from the Northern Hemisphere will interact before reaching AMANDA-II. Combined with the limited overburden above the AMANDA-II detector, this concentrates UHE events at the horizon. This contrasts with the majority of other astrophysical neutrino analyses completed using data from the AMANDA-II detector, which search for neutrinos from the Northern Hemisphere with energies below 10^5 GeV.

The flux of atmospheric neutrinos is negligible at UHE energies, with fewer than 10 events in three years expected from the model in Lipari (1993) after intermediate UHE selection criteria have been applied. This drops to 0.1 events after application of all selection criteria. Similarly, there are fewer than 0.6 events expected in three years at the final selection level from prompt neutrinos from the decay of charmed particles produced in the atmosphere (using the “C” model from Zas et al. (1993)). Therefore, the primary background for the UHE analysis is composed of many lower energy processes that mimic higher energy signal events. Cosmic ray collisions in the upper atmosphere that generate large numbers of nearly parallel muons (or “muon bundles”) can generate high-energy signatures even though the individual muons have much lower energy than single leptons or cascades from UHE neutrinos. Signal and background events spread light over roughly equivalent areas in the detector, but UHE neutrino events are distinguishable because they have higher energy and higher light density than background events. Specialized selection criteria which use these properties, as well as differences in reconstruction variables, separate the UHE neutrinos from the background of muon bundles from atmospheric cosmic rays.

Limits have been placed on the all-flavor neutrino flux in the ultra high-energy range by other experiments (Fig. 3). Additionally, a previous analysis using an earlier configuration of the AMANDA detector called AMANDA-B10, consisting of 302 optical modules (Ackermann et al. 2005), has placed limits on the all-flavor UHE neutrino flux (Fig. 3). This analysis uses 677 optical modules (OMs) of the AMANDA-II detector and gives a combined result using data from three years (2000-2002) with a livetime of 456.8 days.

A description of the AMANDA-II detector is given in section 2. Sections 3 and 4 discuss possible sources of astrophysical neutrinos and background, and the simulation of both. The selection criteria used to separate UHE neutrino signals from background are discussed in section 5. A study of systematic uncertainties is presented in section 6, and the results are shown in section 7.

2. The AMANDA-II Detector

The AMANDA-II detector (Ahrens et al. 2004a) consists of 677 OMs stationed between 1500 m and 2000 m beneath the surface of the Antarctic ice at the geographic South Pole. The OMs are deployed on nineteen vertical cables (called “strings”) arranged in three roughly concentric circles, giving the detector a cylindrical shape with a diameter of approximately 200 m.

Each OM contains a Hamamatsu 8-inch photomultiplier tube (PMT) coupled with silicon gel to a spherical glass pressure housing for continuity of the index of refraction. The OMs are connected to the surface by cables which supply high voltage and carry the signal from the PMT to data acquisition electronics at the surface. The inner ten strings use electrical analog signal transmission, while the outer nine strings primarily use optical fiber transmission (Ahrens et al. 2004a).

The AMANDA-II detector uses a majority trigger of 24 OMs recording a voltage above a set threshold (a “hit”) within a time window of $2.5 \mu\text{s}$. An OM records the maximum amplitude, as well as the leading edge time and time over threshold for each hit, with each OM recording a maximum of eight hits per event. Each photoelectron has approximately a 3% chance of producing an afterpulse caused by ionization of residual gas inside the PMT (Hamamatsu 1999). This afterpulse follows several μs after the generating hit and aids in the detection of UHE events.

AMANDA-II has been collecting data since February 2000. In 2002/2003, waveform digitizers were installed which record the full pulse shape from each OM (Silvestri 2005). In 2005 deployment began on IceCube (Ahrens et al. 2004b), a 1 km^3 array of digital OMs

which now encompasses the AMANDA-II detector.

3. Astrophysical Neutrino and Background Sources

Astrophysical neutrinos with energies in excess of 10^5 GeV may be produced by a variety of sources. A number of theories predict neutrino fluxes from active galactic nuclei (AGN) peaking near 10^6 GeV. In these scenarios, protons are accelerated by the first order Fermi mechanism in shock fronts. In the favored mechanism for neutrino production, these protons interact with the ambient photon field either in the cores (Stecker et al. 1992) or jets (Protheroe 1996; Halzen & Zas 1997; Mannheim et al. 2000; Mannheim 1995) of the AGN and produce neutrinos via the process:

$$p + \gamma \rightarrow \Delta^+ \rightarrow \pi^+[+n] \rightarrow \nu_\mu + \mu^+ \rightarrow \nu_\mu + e^+ + \nu_e + \bar{\nu}_\mu, \quad (1)$$

resulting in a $\nu_e:\nu_\mu:\nu_\tau$ flavor ratio of 1:2:0 at the source¹. The energy spectrum of the neutrinos produced by these interactions generally follows the E^{-2} spectrum of the protons. Theoretical bounds can be placed on the flux of these neutrinos based on the observation of cosmic rays if the p- γ reaction takes place in the jet or other optically thin region of the AGN (Bahcall & Waxman 1998; Mannheim et al. 2000).

UHE neutrinos are also associated with models created to explain the apparent excess of cosmic rays at the highest energies. One scenario involves the decay of massive objects, such as topological defects created by symmetry breaking in the early universe (Sigl et al. 1998). These objects decay close to the Earth into showers of particles, eventually producing neutrinos as well as a fraction of the highest-energy cosmic rays. Z-burst models could also produce some of the highest-energy cosmic rays through the interaction of neutrinos with energies in excess of 10^{13} GeV with relic neutrinos via the Z^0 resonance. Since these neutrino-neutrino interactions are rare, it is possible to directly search for the UHE neutrino fluxes required by this mechanism (Yoshida et al. 1998; Kalashev et al. 2002a). It should be noted that Z-burst scenarios which predict the highest flux of neutrinos have already been eliminated by previous experiments (Barwick et al. 2006). Additionally, Z-burst models predict fluxes of neutrinos which peak at energies above the sensitivity of this analysis or require unrealistic assumptions and are mentioned primarily for completeness.

A guaranteed source of UHE neutrinos comes from the interaction of high-energy cosmic rays with the cosmic microwave background (see e.g. Engel et al. (2001) and Kalashev et al.

¹Neutrino flavor oscillation changes the flavor ratio to 1:1:1 at the Earth. See Kashti & Waxman (2005) for a discussion of different flavor ratios.

(2002b)). However, the flux predictions of these GZK neutrinos are generally several orders of magnitude lower than most of the fluxes listed previously.

The background for this analysis consists of bundles of muons from cosmic rays. The cosmic rays follow an $E^{-2.7}$ spectrum until about 10^6 GeV, where the flux steepens to E^{-3} (Hörandel 2003). They come only from the Southern Hemisphere because bundles from other directions are absorbed by the Earth. According to simulations, there can be as many as 20,000 muons in one bundle spread over a rms cross-sectional area as large as 200 m^2 , and the highest-energy events can deposit energies as large as 2.4×10^6 GeV in the ice around the AMANDA-II detector.

4. Simulation and Experimental Data

UHE neutrinos are simulated using the All Neutrino Interaction Simulation (ANIS) package (Kowalski & Gazizov 2005) to generate and propagate the neutrinos through the Earth. All three flavors of neutrinos are simulated with energies between 10^3 GeV and 10^{12} GeV. The resulting muons and taus are propagated through the rock and ice near the detector using the Muon Monte Carlo (MMC) simulation package (Chirkin & Rhode 2004). Finally, the detector response is simulated using the AMASIM2 simulation package (Hundertmark 1998).

The background muon bundles from cosmic rays are generated using the CORSIKA simulation program with the QGSJET01 hadronic interaction model (Heck 1999). At early levels of this analysis, cosmic ray primaries are generated with composition and spectral indices from Wiebel-Sooth et al. (1999), with energies of the primary particles ranging between 8×10^2 GeV and 10^{11} GeV. At later levels of this analysis, the lower energy primaries have been removed by the selection criteria, and a new simulated data set is used with energy, spectral shape, and composition optimized to simulate high-energy cosmic rays more efficiently. In this optimized simulation, the energy threshold is raised to 8×10^4 GeV and only proton and iron primaries are generated with a spectrum of E^{-2} . These primaries are reweighted following the method outlined in Glasstetter et al. (1999). This optimized simulation is used for level 2 of the analysis and beyond (see Table 1). For 2001 and 2002, the background simulation is further supplemented with the inclusion of a third set of simulated data with the energy threshold increased to 10^6 GeV. For all sets of background simulation, the resulting particles are propagated through the ice using MMC, and the detector response is simulated using AMASIM2.

Data used in this analysis were recorded in the time period between February 2000 and

November 2002, with breaks each austral summer for detector maintenance, engineering, and calibration lasting approximately four months. In addition to maintenance downtime, the detector also has a brief period while recording each event in which it cannot record new events. Runs with anomalous characteristics (such as excessive trigger rates or large numbers of OMs not functioning) are discarded and a method which removes non-physical events caused by short term detector instabilities is applied (Pohl 2004). These factors combine to give a deadtime of 17% of the data taking time for 2000, 22% of the data-taking time for 2001, and 15% of the data taking time for 2002. Additionally, 26 days are excluded from 2000 because the UHE filtered events are polluted with high number of events with incomplete hit information, likely due to a minor detector malfunction. Taking these factors into account, there are 173.5 days of livetime in 2000, 192.5 days of livetime in 2001, and 205.0 days of livetime in 2002. Finally, 20% of the data from each year is set aside for comparison with simulations and to aid in the determination of selection criteria, leading to a total livetime for the three years of 456.8 days.

5. Analysis

Twenty percent of the data from 2000 to 2002 (randomly selected from throughout the three years) is used to test the agreement between background simulations and observations. In order to avoid biasing the determination of selection criteria, this 20% is then discarded, and the developed selection criteria are applied to the remaining 80% of the data. A previous UHE analysis was performed on only the 2000 data using different selection criteria than those described below (see Gerhardt (2005) and Gerhardt (2007) for a more detailed description). For 2001-2002, improved reconstruction techniques such as cascade reconstructions (Ahrens et al. 2003c) were added to the analysis, and the new selection criteria described below were devised in a blind manner. These selection criteria were also applied to the 2000 data to derive a combined three year limit. Due to differences in hit selection for reconstruction between 2000 and 2001-2002, the E^{-2} signal passing rate at the final selection level for the year 2000 is approximately 60% of the rate for the years 2001 and 2002.

In order to maximize the limit setting potential, the selection criteria are initially determined by optimizing the model rejection factor (Hill & Rawlins 2003) given by

$$\text{MRF} = \frac{\bar{\mu}_{90}}{N_{\text{signal}}}, \quad (2)$$

where $\bar{\mu}_{90}$ is 90% confidence level (CL) average event upper limit given by Feldman & Cousins (1998), and N_{signal} is the number of muon neutrinos expected for the signal being tested, in this case an E^{-2} flux. The selection criteria for this analysis are summarized in Table 1 and

described below.

This analysis exploits the differences in total energy and light deposition between bundles of many low-energy muons and single UHE muons or cascades from UHE neutrinos. UHE neutrinos deposit equal or greater amounts of light in the ice than background muon bundles. In addition to being lower energy, background muon bundles spread their light over the cross sectional area of the entire muon bundle, rather than just along a single muon track or into a single cascade. Both signal and background events can have a large number of hits in the array, but for the same number of hit OMs, the muon bundle has a lower total number of hits, NHITS (recall each OM may have multiple separate hits in one event; see Fig. 4). The number of hits for UHE neutrinos is increased by the tendency of bright signals to produce afterpulses in the PMT. Background muon bundles also have a higher fraction of OMs with a single hit (F1H), while a UHE neutrino generates more multiple hits (Fig. 5). The F1H variable is correlated with energy (Fig. 6) and is effective at removing lower energy background muon bundle events. The level 1 and 2 selection criteria require that $\text{NHITS} > 140$ and $\text{F1H} < 0.53$ and reduce the background by a factor of 2×10^3 relative to trigger level (level 0 on Tables 2 and 3).

At this point the data sample is sufficiently reduced that computationally intensive reconstructions become feasible. Reconstruction algorithms used in this analysis employ a maximum likelihood method which takes into account the absorption and scattering of light in ice. For muons, the reconstruction compares time residuals to those expected from a Cherenkov cone for a minimally ionizing muon (Ahrens et al. 2004a), while the cascade reconstruction uses Cherenkov light from an electromagnetic cascade for comparison (Ahrens et al. 2003c). Reconstructions which are optimized for spherical (cascade) depositions of light are used to distinguish UHE neutrinos from background muon bundles which happen to have a large energy deposition, such as a bremsstrahlung or $e^+ e^-$ pair creation, inside the detector fiducial volume.

Before application of the level 3 selection criteria, the data sets are split into “cascade-like” and “muon-like” subsets. This selection is performed using the negative log likelihood of the cascade reconstruction (L_{casc} , see Fig. 7), where events with a $L_{\text{casc}} < 7$ are considered “cascade-like.”

5.1. “Cascade-like” Events

Background events in the “cascade-like” subset are characterized by either a large light deposition in or very near the instrumented volume of AMANDA-II or a path which clips

the top or bottom of the array. In either case, the energy deposition is significantly less than the energy deposited by a UHE neutrino, allowing application of selection criteria which correlate with energy. One of these is $F1H_{ELEC}$ (Fig. 8), a variable similar to the $F1H$ variable described above, except that it uses only OMs whose signal is brought to the surface by electrical cables. The signal spreads as it propagates up the cable, causing hits close together in time to be combined. This gives $F1H_{ELEC}$ a different distribution from $F1H$, and both variables are good estimators of energy deposited inside the detector (Fig. 6). Additionally, the fraction of OMs with exactly four hits ($F4H$) is another useful energy indicator. The value of four hits was chosen as a compromise between the number of hits expected from OMs with electrical cables and OMs with optical fibers. OMs with optical fibers typically have more hits than OMs with electrical cables because very little pulse spreading occurs as the signal propagates up the fiber. The level 3 selection criteria uses the output of a neural net with $F1H_{ELEC}$, $F4H$, and $F1H$ as input variables (Fig. 9). As selection levels 4 and 5, separate applications of the $F4H$ and $F1H_{ELEC}$ variables remove persistent lower energy background events.

The remaining background muon bundles have a different hit distribution than UHE neutrinos. In the background muon bundles, a large light deposition can be washed out by the continuous, dimmer light deposition from hundreds to tens of thousands of muons tracks. In contrast, UHE muons can have one light deposition that is several orders of magnitude brighter than the light from the rest of the muon track and looks very similar to bright cascades from UHE electron and tau neutrinos. For all cases, the initial cascade reconstruction is generally concentric with this large energy deposition, so ignoring OMs that are within 60 m of the initial cascade reconstruction reduces the fraction of OMs that are triggered with photons from the cascade. For background, the remaining light will be dominated by light depositions from the tracks of the muon bundles and be less likely to reconstruct as a cascade. In contrast, signal events, with their energetic cascades, will still appear cascade-like and reconstruct with a better likelihood (L_{60}). The final selection criteria for “cascade-like” events (chosen by optimizing the MRF) requires that these events be well reconstructed by a cascade reconstruction performed using only OMs with distances greater than 60 m and reduces the background expectation to 0 events for this subset.

The number of events at each selection level for experiment, background, and signal simulation for the “cascade-like” subset are shown in Table 2.

5.2. “Muon-like” Events

Background events in the “muon-like” subset are characterized by more uniform, track-like light deposition and are more easily reconstructed by existing reconstruction algorithms than “cascade-like” events. A reconstruction algorithm based on parameterization of time residuals from simulated muon bundles is used to reconstruct the zenith angle of the events (Fig. 10). Since most background muon bundles will come from a downgoing direction, while UHE neutrinos will come primarily from the horizontal direction (Klein & Mann 1999), requiring that the zenith angle $> 85^\circ$ (where a zenith angle of 90° is horizontal) reduces the background by a factor of 30. The remaining background in the “muon-like” subset are misreconstructed events, since the actual flux close to the horizon is very small. A reconstruction based on the hit pattern of a Cherenkov cone for a minimally ionizing muon is applied to these events (Ahrens et al. 2004a). Selecting only well-reconstructed events using the likelihood of this reconstruction (L_{muon}) is sufficient to remove all background events in this subset. The value of this selection criteria was initially chosen to optimize the MRF for muon neutrinos with an E^{-2} spectrum. However, by increasing the selection value slightly beyond the value which gave the minimum MRF, all background events were rejected with only a few percent drop in the sensitivity (Fig. 11). Since the uncertainty in the cosmic ray spectrum is very large at these energies, the more stringent selection criterion was applied to correct for the fact that the MRF is optimized without uncertainties.

The number of events at each selection level for experiment, background, and signal simulation for the “muon-like” subset are shown in Table 3.

6. Statistical and Systematic Uncertainties

Because there is no test beam which can be used to determine the absolute sensitivity of the AMANDA-II detector, calculations of sensitivity rely on simulation. The dominant sources of statistical and systematic uncertainty in this calculation are described below. The systematic uncertainties are assumed to have a flat distribution and are summed in quadrature separately for background and signal. The uncertainties have been included into the final limit using the method described in Tegenfeldt & Conrad (2005).

6.1. Uncertainties Due to Limited Simulation Statistics

Due to computational requirements, background simulation statistics are somewhat limited. Ideally, one would scale the statistical uncertainty on zero events based on the simula-

tion event weights in nearby non-zero bins. However, the optimized background simulations used in this analysis have large variations in event weights approaching this region, making determination of this factor difficult. Nevertheless, the statistical uncertainties near the edge of the distribution are on the order of the uncertainties for a simulation with a livetime equivalent to the data taking period, so no scaling factor is applied to the statistical uncertainty. A statistical uncertainty of 1.29, the 1σ Feldman-Cousins event upper limit on zero observed events (Feldman & Cousins 1998), is assumed at the final selection level. Signal simulation has an average statistical uncertainty of 5% for each neutrino flavor.

6.2. Normalization of Cosmic Ray Flux

The average energy of cosmic ray primaries at the penultimate selection level is 4.4×10^7 GeV, which is considerably above the knee in the all-particle cosmic ray spectrum. Numerous experiments have measured a large spread in the absolute normalization of the flux of cosmic rays at this energy (see Kampert (2007) for a recent review). Estimates of the uncertainty in the normalization of the cosmic ray flux range from 20% (Hörandel 2003) to a factor of two (Particle Data Group 2006). This analysis uses the more conservative uncertainty of a factor of two.

6.3. Cosmic Ray Composition

There is considerable uncertainty in the cosmic ray composition above the knee (Particle Data Group 2006). We estimate the systematic uncertainty by considering two cases: proton-dominated composition and iron-dominated composition. The simulated background cosmic ray flux is approximated by separately treating proton and iron primaries combined in a total spectrum that becomes effectively iron-dominated above 10^7 GeV using the method described in Glasstetter et al. (1999). The iron-dominated spectrum yields a 30% higher background event rate than the rate from a proton-dominated spectrum at the penultimate selection level. This value of 30% is used as the uncertainty due to the cosmic ray composition.

6.4. Detector Sensitivity

The properties of the refrozen ice around each OM, the absolute sensitivity of individual OMs, and obscuration of OMs by nearby power cables can effect the detector sensitivity. This analysis uses the value obtained in Ahrens et al. (2003a) where reasonable variations

of these parameters in the simulation were found to cause a 15% variation in the E^{-2} signal and background passing rate.

6.5. Implementation of Ice Properties

As photons travel through the ice they are scattered and absorbed. The absorption and scattering lengths of the ice around the AMANDA-II detector have been measured very accurately using in situ light sources (Ackermann et al. 2006). Uncertainties are introduced due to the limited precision with which these parameters are included in the simulation. Varying the scattering and absorption lengths in the detector simulation by 10% were found to cause a difference in number of expected signal events (for an E^{-2} spectrum) of 34% (Ackermann et al. 2005), which is used as a conservative estimate of the uncertainty due to implementation of ice properties. If too large of a deviation in background rate relative to the experimental rate was observed for a set of ice property parameters, the background rate was normalized to the experimental rate, and the signal rate was scaled accordingly. This was done to ensure that the variation in absorption and scattering lengths covered a reasonable range of ice properties.

6.6. Neutrino Cross Section

The uncertainty in the standard model neutrino cross section has been quantified recently (Anchordoqui et al. 2006) taking into account the experimental uncertainties on the parton distribution functions measured at HERA (Chekanov et al. 2005), as well as theoretical uncertainties in the effect of heavy quark masses on the parton distribution function evolution and on the calculation of the structure functions. The corresponding maximum variation in the number of expected signal events (for an E^{-2} spectrum) is 10%, in agreement with previous estimates (Ackermann et al. 2005).

Screening effects are expected to suppress the neutrino-nucleon cross section at energies in excess of 10^8 GeV (see e.g. Kutak & Kwiecinski (2003); Berger et al. (2007)). This has a negligible effect on the number of signal events expected for an E^{-2} spectrum because the majority of signal is found below these energies (Fig. 12). Even if the suppression is as extreme as in the Colour Glass Condensate model (Henley & Jalilian-Marian 2005), the event rate decreases by only 11%.

6.7. Differences in Simulated Distributions

An examination of the L_{muon} distribution for the “muon-like” subset after level 3 of this analysis suggests the background simulation is shifted by one bin relative to the experiment (Fig. 13). Shifting all simulation distributions to the left by one bin leads to better agreement between the background simulation and experimental distributions and an increase in 8% in the number of expected signal events for an E^{-2} spectrum.

6.8. The Landau-Pomeranchuk-Migdal (LPM) Effect

At ultra high-energies, the LPM effect suppresses the bremsstrahlung cross section for electrons and the pair-production cross section of photons created in a cascade by an electron neutrino (Landau & Pomeranchuk 1953; Migdal 1957). This lengthens the resultant shower produced by a factor that goes as \sqrt{E} . Above 10^8 GeV, the extended shower length becomes comparable to the spacing between OMs on a string (Klein 2004). Additionally, as the LPM effect suppresses the bremsstrahlung and pair productions cross sections, photonuclear and electronuclear interactions begin to dominate which lead to the production of muons inside the electromagnetic cascade. Toy simulations were performed which superimposed a muon with an energy of 10^5 GeV onto a cascade with energy of 10^8 GeV. While the addition of the muon shifted the L_{casc} distribution 5% towards higher (more “muon-like”) values, the resulting events still passed all selection criteria indicating that the effects of muons created inside cascades are negligible.

The LPM effect is not included in the simulations of electron neutrinos, but it can be approximated by excluding all electron neutrinos with energies in excess of 10^8 GeV. This is an overestimation of the uncertainty introduced by the LPM effect, as extended showers may manifest as several separate showers which are likely to survive all selection criteria and the addition of low-energy muons is not expected to significantly alter the UHE cascade light deposition. Neglecting electron neutrinos with energies in excess of 10^8 GeV reduces the number of expected signal events by 2% for an E^{-2} spectrum.

6.9. Summary of Uncertainties

The systematic errors are shown in Table 4. Summing the systematic errors of the signal simulation in quadrature gives a systematic uncertainty of $\pm 39\%$. Combining this with the statistical uncertainty of 5% per neutrino flavor gives a total maximum uncertainty of 40%. Following a similar method for the background simulation, the systematic uncertainty is

+101% / -60%. Scaling the statistical uncertainty of the background simulation by the systematic uncertainty gives a maximum background expectation of fewer than 2.6 events for three years.

7. Results

After applying all selection criteria, no background events are expected for 456.8 days. Incorporating the statistical and systematic uncertainties, the background is expected to be found with a uniform prior probability between 0 and 2.6 events. A possible sensitivity calculation which incorporates these uncertainties can be generated by assuming a flat prior with a mean of 1.3 events and a corresponding data expectation of 1 event. This gives a 90% CL event upper limit of 3.5 (Tegenfeldt & Conrad 2005) and a sensitivity of 1.8×10^{-7} GeV cm⁻² s⁻¹ sr⁻¹, with the central 90% of the E⁻² signal found in the energy range 2×10^5 GeV to 10^9 GeV. Table 5 shows the expected number of each flavor of UHE neutrino passing the final selection level for a $10^{-6} \times E^{-2}$ flux. The energy spectra of each flavor are shown in Fig. 12.

Two events are observed in the data sample at the final selection level (Fig. 13), while fewer than 2.6 background events are expected which gives a 90% CL average event upper limit of 5.3. After applying all selection criteria, 20 events are expected for a $10^{-6} \times E^{-2}$ all flavor flux (Table 5). The upper limit on the all-flavor neutrino flux (assuming a 1:1:1 $\nu_e : \nu_\mu : \nu_\tau$ flavor ratio) is

$$E^2 \Phi_{90\%CL} \leq 2.7 \times 10^{-7} \text{GeV cm}^{-2} \text{s}^{-1} \text{sr}^{-1}, \quad (3)$$

including systematic uncertainties, with the central 90% of the E⁻² signal found between the energies of 2×10^5 GeV and 10^9 GeV.

A number of theories which predict fluxes with non-E⁻² spectral shapes (Fig. 3) were also tested by reweighting the simulated signal. These include the hidden-core AGN model of Stecker et al. (1992) which has been updated to reflect a better understanding of AGN emission (Stecker 2005), as well as AGN models in which neutrinos are accelerated in optically thin regions (Protheroe 1996; Halzen & Zas 1997; Mannheim 1995; Mannheim et al. 2000). Including uncertainties, this analysis restricts at a 90% CL the AGN models from Halzen & Zas (1997) and Mannheim et al. (2000). Also the previously rejected (Ackermann et al. 2005) models from Protheroe (1996) and Stecker et al. (1992) are rejected at the 90% CL by this analysis (see Fig. 14 and Table 6). The model by Stecker et al. (1992) builds on a correlation between X-rays and neutrinos from AGNs. Other models using the same correlation give a similar normalization and violate current limits by an order of magnitude as

well. As previously pointed out by Becker et al. (2007), such a correlation can be excluded.

While we do not directly exclude the flux from the Stecker (2005) hidden-core AGN model, it is possible to set limits on the parameters used in the model. In this model, the flux of neutrinos is normalized to the extragalactic MeV photon flux measured by COMPTEL with the assumption that the flux of photons from Seyfert galaxies is responsible for 10% of this MeV background. If the neutrino flux scales linearly with the photon flux, then the maximum contribution of hidden-core AGNs, such as Seyfert galaxies, to the extragalactic MeV photon flux must be less than 29%.

Fluxes of neutrinos from the decay of topological defects (Sigl et al. 1998) and the UHE fluxes required for the Z-bursts mechanism (Yoshida et al. 1998; Kalashev et al. 2002a) peak at too high of an energy to be detected by this analysis. Neutrinos from the interaction of cosmic rays with cosmic microwave background photons are produced at too low of a flux for this analysis to detect (see Table 6).

The number of expected events of a given flavor (ν and $\bar{\nu}$) for spectra not tested in this paper can be calculated using the formula

$$N_{signal} = T \int dE_{\nu} d\Omega \Phi_{\nu}(E_{\nu}) A_{eff}^{\nu}(E_{\nu}), \quad (4)$$

where T is the total livetime (456.8 days), A_{eff}^{ν} is the angle averaged neutrino effective area (Fig. 15), and Φ_{ν} is the flux at the Earth's surface.

8. Conclusion

The diffuse neutrino flux limit for a 1:1:1 $\nu_e : \nu_{\mu} : \nu_{\tau}$ flavor ratio set by this analysis of

$$E^2 \Phi_{90\%CL} \leq 2.7 \times 10^{-7} \text{GeV cm}^{-2} \text{s}^{-1} \text{sr}^{-1}, \quad (5)$$

is the most stringent to date above 10^5 GeV. A number of models for neutrino production have been rejected (see Table 6 for a full list). AMANDA-II hardware upgrades which were completed in 2003 should lead to an improvement of the sensitivity at ultra high-energies (Silvestri 2005). Additionally, AMANDA-II is now surrounded by the next-generation IceCube detector which is currently under construction. The sensitivity to UHE muon neutrinos for 1 year is expected to increase by roughly an order of magnitude as the IceCube detector approaches its final size of 1 km^3 (Ahrens et al. 2004b).

We acknowledge the support from the following agencies: National Science Foundation-Office of Polar Program; National Science Foundation-Physics Division; University of Wis-

consin Alumni Research Foundation; Department of Energy, and National Energy Research Scientific Computing Center (supported by the Office of Energy Research of the Department of Energy); the NSF-supported TeraGrid system at the San Diego Supercomputer Center (SDSC); the National Center for Supercomputing Applications (NCSA); Swedish Research Council; Swedish Polar Research Secretariat; Knut and Alice Wallenberg Foundation, Sweden; German Ministry for Education and Research; Deutsche Forschungsgemeinschaft (DFG), Germany; Fund for Scientific Research (FNRS-FWO); Flanders Institute to encourage scientific and technological research in industry (IWT); Belgian Federal Office for Scientific, Technical and Cultural affairs (OSTC); the Netherlands Organisation for Scientific Research (NWO); M. Ribordy acknowledges the support of the SNF (Switzerland); A. Kappes and J. D. Zornoza acknowledges the Marie Curie OIF Program; L. Gerhardt acknowledges the support of the University of California, Irvine MPC Computational Cluster and Achievement Rewards for College Scientists (ARCS).

REFERENCES

- Achterberg, A. et al., 2007 Phys. Rev. D, in press (arXiv:0705.1315).
- Ackermann, M. et al., 2004, Astroparticle Physics, 22, 127.
- Ackermann, M. et al., 2005, Astroparticle Physics, 22, 339.
- Ackermann, M. et al., 2006, Journal of Geophysical Research, 3, D13203.
- Ahlers, M. et al., 2005, Phys. Rev. D, 72, 023001.
- Ahrens, J. et al., 2003, Astrophys. Journal, 583, 1040.
- Ahrens, J. et al., 2003, Phys. Rev. Lett., 90, 251101.
- Ahrens, J. et al., 2003, Phys. Rev. D, 67, 012003.
- Ahrens, J. et al., 2004, Nuclear Instruments and Methods A, 524, 169.
- Ahrens, J. et al., 2004, Astroparticle Physics, 20, 507.
- Anchordoqui, L., Cooper-Sakar, A., Hooper D., and, Sakar, S., 2006, Phys, Rev. D, 74, 043008.
- Aynutdinov, V. et al., 2006, Astroparticle Physics, 140.
- Bahcall, J. and Waxman, E., 1998, Phys. Rev. D, 59, 023002.

- Barwick, S. et al., 2006, Phys. Rev. Lett., 96, 171101.
- Becker, J. K., Groß, A., Münich, K., Dreyer, J., Rhode, W. and Biermann, P. L., 2007, Astroparticle Physics, in press (astro-ph/0607427).
- Berger, E., Block, M., McKay, D., and Tan, C., 2007, preprint (hep-ph/0708.1960v1).
- Chekanov, S. et al., 2005, European Physical Journal C, 42, 1.
- Chirkin, D. and Rhode, W., 2004, preprint (hep-ph/0407075).
- Engel, R., Seckel, D., and Stanev T., 2001, Phys. Rev. D, 64, 093010. Curve shown for $\Lambda=0.7$, taken from ftp://ftp.bartol.udel.edu/seckel/ess-gzk/flux_n3_8_flat_om0p3.txt.
- Feldman, G. and Cousins, F., 1998, Phys. Rev. D, 57, 3873.
- Gandhi, R., Quigg, C., Reno, M., and Sarcevic, I., 1998, Phys. Rev. D, 58, 093009.
- Gerhardt, L., 2005, Proc. 29th Int. Cosmic Ray Conf., Pune, India, 111 (astro-ph/0509330).
- Gerhardt, L., 2007, Proc. 14th Int. Conf. on Supersymmetry and the Unification of Fundamental Interactions, AIP Conf. Proc. 903, 622.
- Glasstetter, R. et al., 1999, Proc. 26th Int. Cosmic Ray Conf., Utah, USA, 1, 222.
- Halzen, F. and Zas, E., 1997, Astrophys. Journal, 488, 669.
- Hamamatsu, 1999, Photomultiplier Tubes, Basics and Applications, second ed.
- Heck, D., 1999, DESY-PROC-1999-01, 227.
- Henley, E. and Jalilian-Marian, J., 2005, preprint (hep-ph/0512220v1).
- Hill, G. and Rawlins, K., 2003, Astroparticle Physics, 19, 393.
- Hörandel, J., 2003, Astroparticle Physics, 19, 193.
- Hundertmark, S., 1998, Proc. 1st Workshop Methodical Aspects of Underwater/Ice Neutrino Telescopes, Zeuthen, Germany.
- Kalashov, O. et al., 2002, Phys. Rev. D 65, 103003.
- Kalashov, O. et al., 2002, Phys. Rev. D 66, 063004.
- Kampert, K.-H., 2007, Nuclear Physics B (Proc. Suppl.), 165, 294.

- Kashti, T. and Waxman, E. Phys. Rev. Lett. 95, 181101.
- Klein, J. and Mann, A., 1999, Astroparticle Physics 10, 321.
- Klein, S., 2004, preprint (astro-ph/0412546v1).
- Kowalski, M. and Gazizov, A., 2005, Computer Physics Communications, 172, 203.
- Kravchenko, I. et al., 2006, Phys. Rev. D, 73, 082002.
- Kutak, K. and Kwieciński, J., 2003, preprint (hep-ph/0303209v4).
- Landau, L. and Pomeranchuk, I., 1953, Dok. Akad. Nauk SSSR, 92, 535.
- Lipari, P., 1993, Astroparticle Physics, 1, 195.
- Mannheim, K., 1995, Astroparticle Physics, 3, 295.
- Mannheim, K., Protheroe, R. J., and Rachen, J., 2000, Phys. Rev. D, 63, 023003.
- Migdal, A., 1957, JETP, 5, 527.
- Particle Data Group, 2006, Journal of Phys. G. 33, 1.
- Pohl A.C., 2004, Licenciate thesis, Kalmar University.
- Protheroe, R., 1996, preprint (astro-ph/9607165).
- Silvestri, A., 2005, Proc. 29th Int. Cosmic Ray Conf., Pune, India, 431.
- Stecker, F., 2005, Phys. Rev. D, 72, 107301.
- Stecker, F., Done, C., Salamon, M., and Sommers, P., 1992, Phys. Rev. Lett., 69, 2738.
- Sigl, G., Lee, S., Bhattacharjee, P., and Yoshida, S., 1998, Phys. Rev. D, 59, 043504.
- Tegenfeldt, F. and Conrad, J., 2005, Nuclear Instruments and Methods in Physics Research A, 539, 407.
- Wiebel-Sooth, B., Biermann, P., and Meyer, H., 1999, col. VI/3c, Springer Verlag, 37.
- Yoshida, S., Sigl, G., and Lee S., 1998, Phys. Rev. Lett., 81, 5505.
- Zas, E., Halzen, F., and Vázquez, R., 1993, Astroparticle Physics, 1, 297.

Table 1: Selection criteria.

Level	Selection Criteria	
0	Hit Cleaning and Retriggering	
1	F1H < 0.72	
	NHITS > 140	
2	F1H < 0.53	
	“Cascade-like”	“Muon-like”
3	$L_{\text{casc}} < 7$	$L_{\text{casc}} \geq 7$
	Neural Net > 0.93	Zenith Angle > 85
4	F4H < 0.1	$L_{\text{muon}} < 6.9$
5	$F1H_{\text{ELEC}} < 0.56$	-
6	$L_{60} < 6.6$	-

Table 2: Number of experimental, simulated background, and simulated signal events in the “cascade-like” subset at each selection level for 456.8 days.

Level	Data	BG Simulation	Signal Simulation
0	2.7×10^9	$1.8_{-1.1}^{+1.8} \times 10^9$	621.7
1	3.9×10^7	$3.1_{-1.8}^{+3.1} \times 10^7$	270.8
2	1.7×10^4	$1.4_{-0.8}^{+1.4} \times 10^4$	89.2
3	155	62_{-37}^{+63}	32.0
4	151	61_{-37}^{+62}	31.0
5	46	32_{-19}^{+32}	27.1
6	0	$0^{+2.6}$	16.0

Note. — Levels 0 and 1 show combined numbers for both “muon-like” and “cascade-like” subsets. Signal is shown with a low energy threshold of 10^4 GeV for a neutrino spectrum of $dN/dE = 10^{-6} \times E^{-2} \text{ GeV}^{-1} \text{ cm}^{-2} \text{ s}^{-1} \text{ sr}^{-1}$, with an assumed 1:1:1 $\nu_e : \nu_\mu : \nu_\tau$ flavor ratio. Values at selection level 0 and 1 for data and background simulation are extrapolated from the 2000 datasets. The background simulation is shown with systematic and statistical uncertainties described in Section 6. The number of “muon-like” events are shown in Table 3.

Table 3: Number of experimental, simulated background, and simulated signal events in the “muon-like” subset at each selection level for 456.8 days.

Level	Data	BG Simulation	Signal Simulation
0	2.7×10^9	$1.8_{-1.1}^{+1.8} \times 10^9$	621.7
1	3.9×10^7	$3.1_{-1.8}^{+3.1} \times 10^7$	270.8
2	1.4×10^6	$9.0_{-5.4}^{+9.1} \times 10^5$	85.2
3	4.6×10^4	$2.7_{-1.6}^{+2.7} \times 10^4$	57.9
4	2	$0^{+2.6}$	4.0

Note. — Levels 0 and 1 show combined numbers for both “muon-like” and “cascade-like” subsets. Signal is shown with a low energy threshold of 10^4 GeV for a neutrino spectrum of $dN/dE = 10^{-6} \times E^{-2} \text{ GeV}^{-1} \text{ cm}^{-2} \text{ s}^{-1} \text{ sr}^{-1}$, with an assumed 1:1:1 $\nu_e : \nu_\mu : \nu_\tau$ flavor ratio. Values at selection level 0 and 1 for data and background simulation are extrapolated from the 2000 datasets. The background simulation is shown with systematic and statistical uncertainties described in Section 6. The number of “cascade-like” events are shown in Table 2.

Table 4: Simulation Uncertainties

Source	BG Sim	Sig Sim
Cosmic Ray Normalization	+100% / -50%	-
Cosmic Ray Composition	-30%	-
Detector Sensitivity	$\pm 15\%$	$\pm 15\%$
Ice Properties	-	$\pm 34\%$
Neutrino Cross Section	-	$\pm 10\%$
Simulation Distribution	-	+8%
LPM Effect	-	-2%
Total	+101% / -60%	+39% / -39%

Table 5: Number of simulated neutrino events in the “cascade-like” and “muon-like” subsets passing all selection criteria for three years for a neutrino spectrum of $d(N_{\nu_e} + N_{\nu_\mu} + N_{\nu_\tau})/dE = 10^{-6} \times E^{-2} \text{ GeV}^{-1} \text{ cm}^{-2} \text{ s}^{-1} \text{ sr}^{-1}$.

Neutrino Flavor	“Cascade-like”	“Muon-like”	Total
Electron	7.7	0.1	7.8
Muon	3.9	3.6	7.5
Tau	4.4	0.3	4.7
All Flavors	16.0	4.0	20.0

Table 6: Flux models, the number of neutrinos of all flavors expected at the Earth at the final selection level, and the MRFs for 456.8 days of livetime.

Model	ν_{all}	MRF	Reference
AGN ^a	20.6	0.3	(Protheroe 1996)
AGN ^a	17.4	0.3	(Stecker et al. 1992)
AGN ^a	8.8	0.6	(Halzen & Zas 1997)
AGN ^a	5.9	0.9	(Mannheim et al. 2000)
AGN RL B ^a	4.5	1.2	(Mannheim 1995)
Z-burst	2.0	2.7	(Kalashev et al. 2002a)
AGN	1.8	2.9	(Stecker 2005)
GZK ν norm AGASA ^b	1.8	2.9	(Ahlers et al. 2005)
GZK ν mono-energetic	1.2	4.4	(Kalashev et al. 2002b)
GZK ν a=2	1.1	4.8	(Kalashev et al. 2002b)
GZK ν norm HiRes ^b	1.0	5.3	(Ahlers et al. 2005)
TD	0.9	5.9	(Sigl et al. 1998)
AGN RL A ^a	0.3	18.0	(Mannheim 1995)
Z-burst	0.1	53.0	(Yoshida et al. 1998)
GZK ν	0.06	88.0	(Engel et al. 2001)

^aThese values have been divided by two to account for neutrino oscillation from a source with an initial 1:2:0 $\nu_e:\nu_\mu:\nu_\tau$ flux.

^bLower energy threshold of 10^7 GeV applied.

Note. — A MRF of less than one indicates that the model is excluded with 90% confidence.

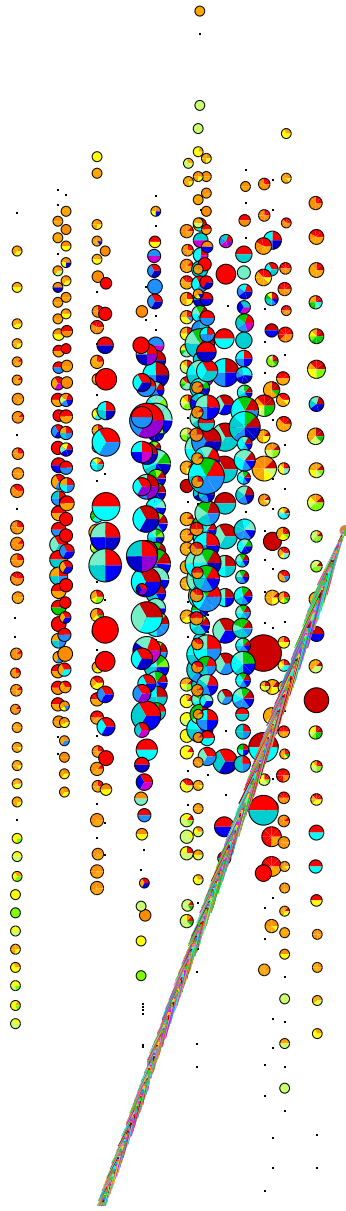


Fig. 1.— Simulated muon neutrino event with an energy of 3.8×10^8 GeV. The muon passes roughly 70 m outside the instrumented volume of the detector. Colored circles represent hit OMs. The color of the circle indicates the hit time (red is earliest), with multiple colors indicating multiple hits in that OM. The size of the circle is correlated with the number of photons produced.

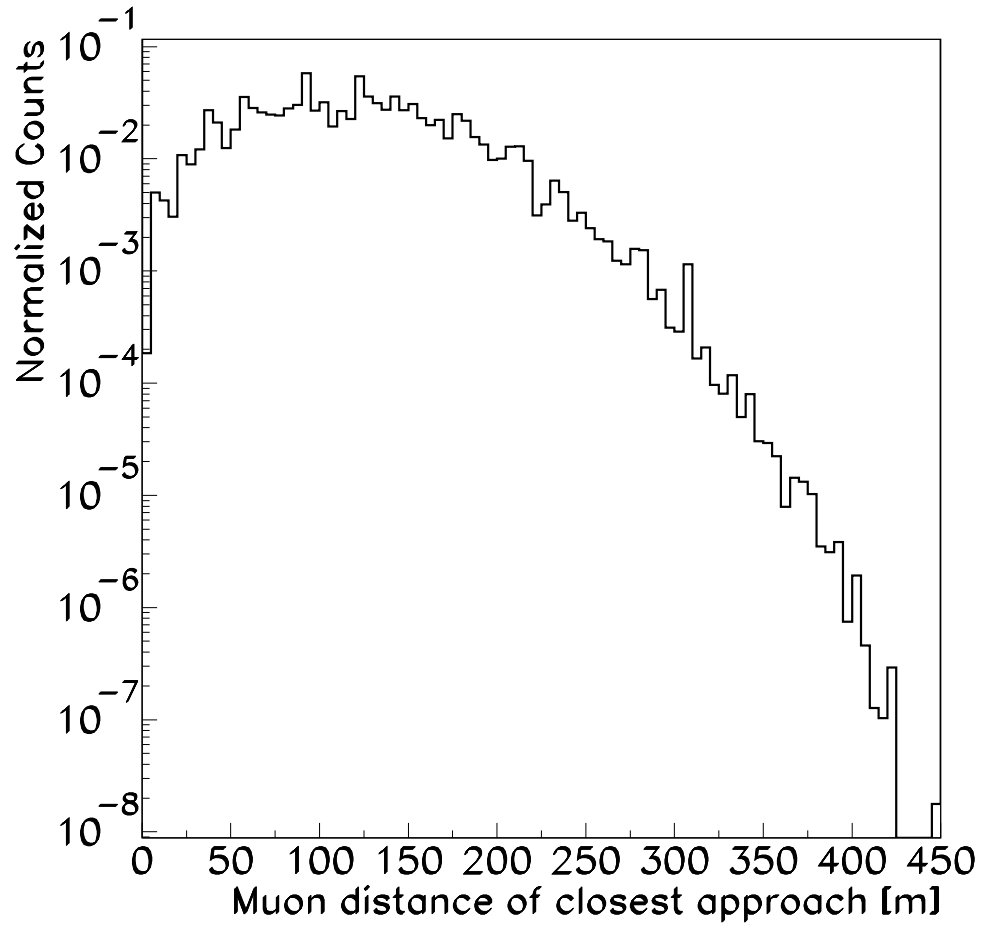


Fig. 2.— Distance of closest approach to the detector center for muons from UHE muon neutrinos (shown with an E^{-2} spectrum) which pass all selection criteria of this analysis.

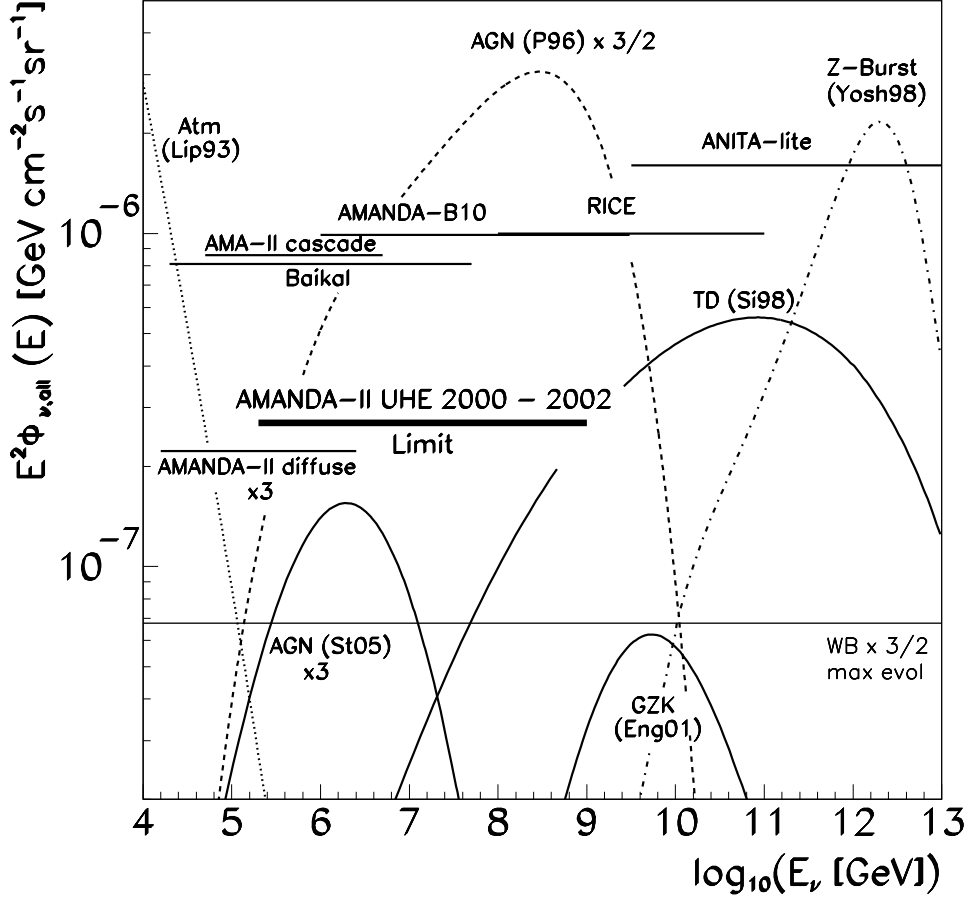


Fig. 3.— All-flavor UHE neutrino flux limit for 2000-2002 over the range which contains the central 90% of the expected signal with an E^{-2} spectrum. Also shown are several representative models: St05 from Stecker (2005) multiplied by 3, P96 from Protheroe (1996) multiplied by 3/2, Eng01 from Engel et al. (2001), Si98 from Sigl et al. (1998), Yosh98 from Yoshida et al. (1998), Lip93 from Lipari (1993), and the Waxman-Bahcall upper bound (Bahcall & Waxman 1998) multiplied by 3/2. Existing experimental limits shown are from the RICE (Kravchenko et al. 2006), ANITA-lite (Barwick et al. 2006), and Baikal (Aynutdinov et al. 2006) experiments, the UHE limit from AMANDA-B10 (Ackermann et al. 2005), the lower-energy diffuse muon limit multiplied by 3 (Achterberg et al. 2007) and cascade limit (Ackermann et al. 2004) from AMANDA-II.

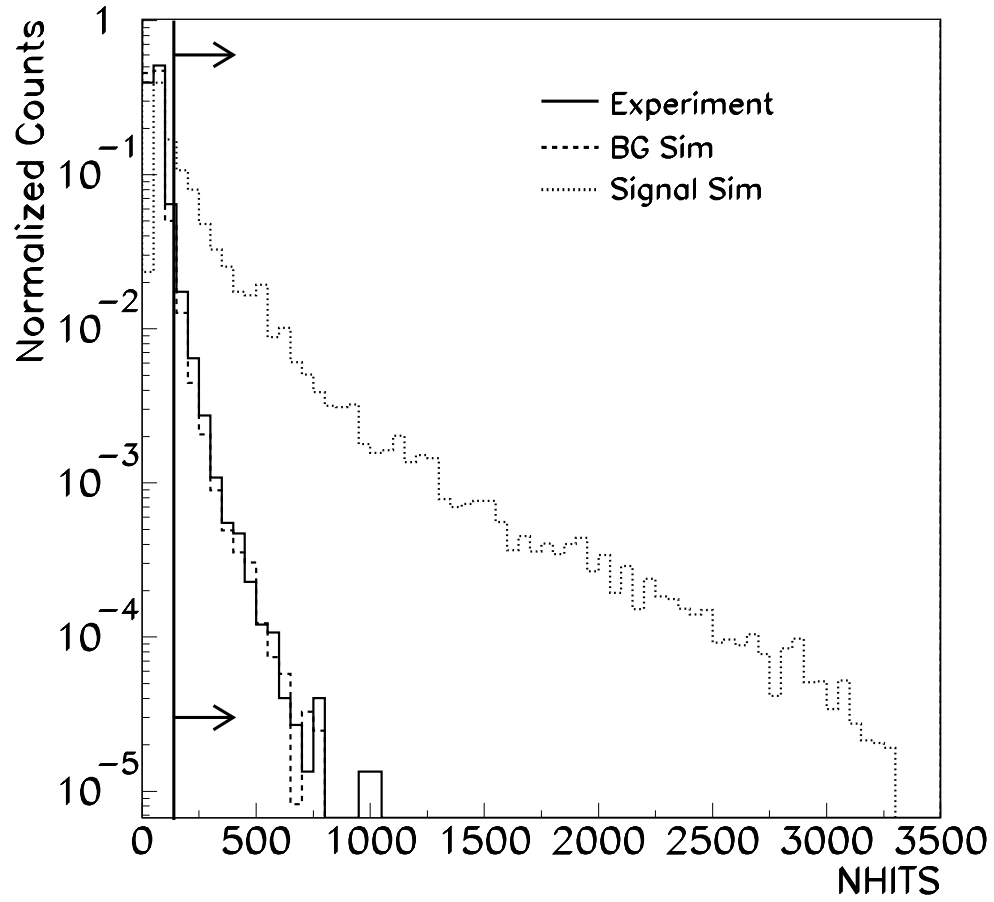


Fig. 4.— NHITS distribution for the experiment, background, and E^{-2} muon neutrino signal simulations before level 1 of this analysis.

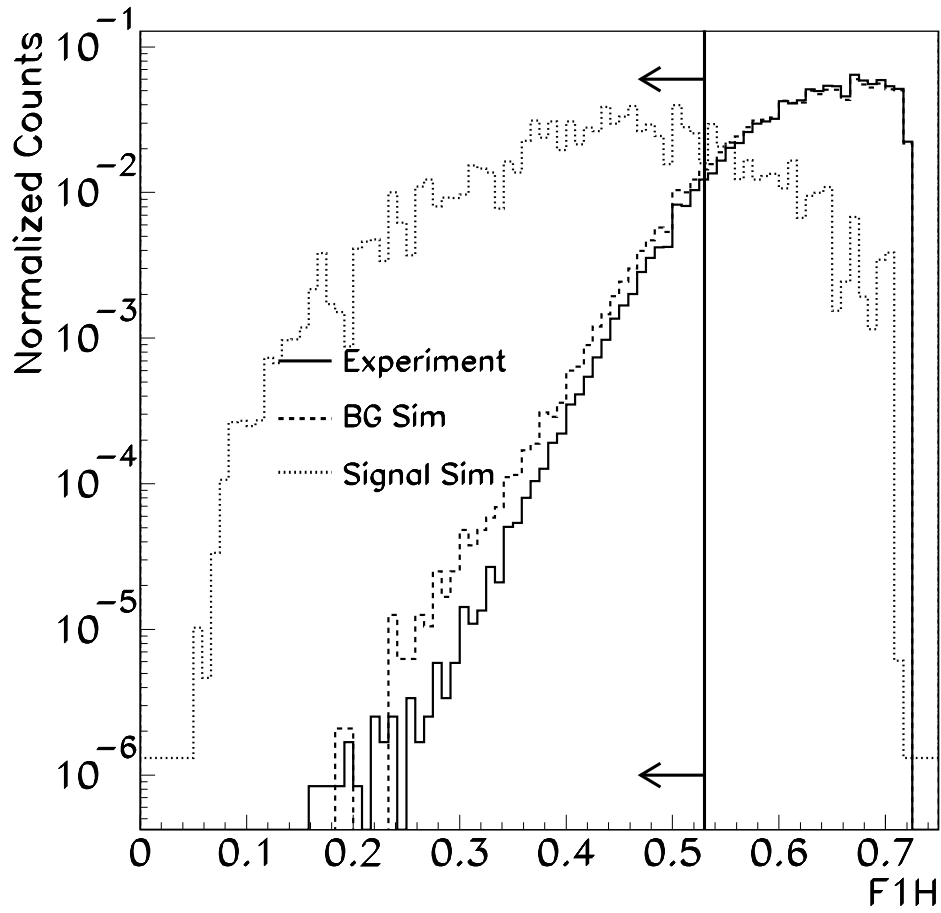


Fig. 5.— Distribution of F1H (the fraction of OMs with a single hit) for the experiment, background, and E^{-2} muon neutrino signal simulations after level 1 of this analysis. The average F1H drops with energy (see Fig. 6).

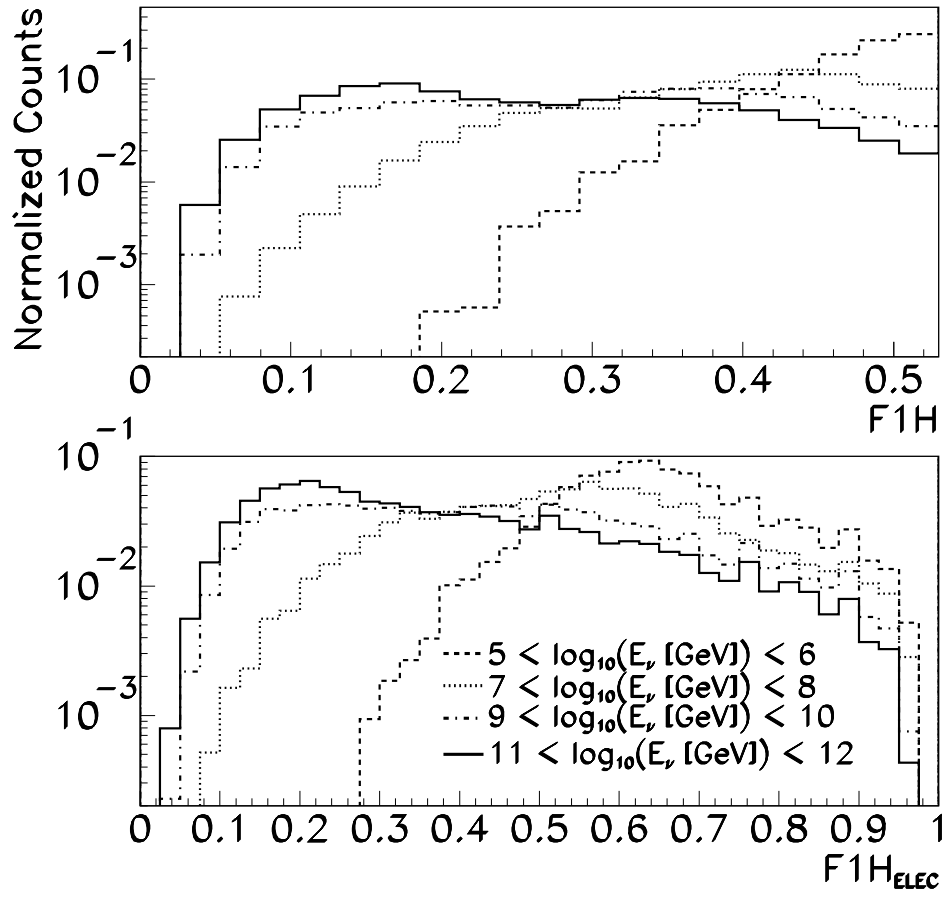


Fig. 6.— F1H (top) and F1H_{ELEC} (bottom) distributions for various energy decades of muon neutrino signal. These variables serve as rough estimator of energy for the UHE analysis.

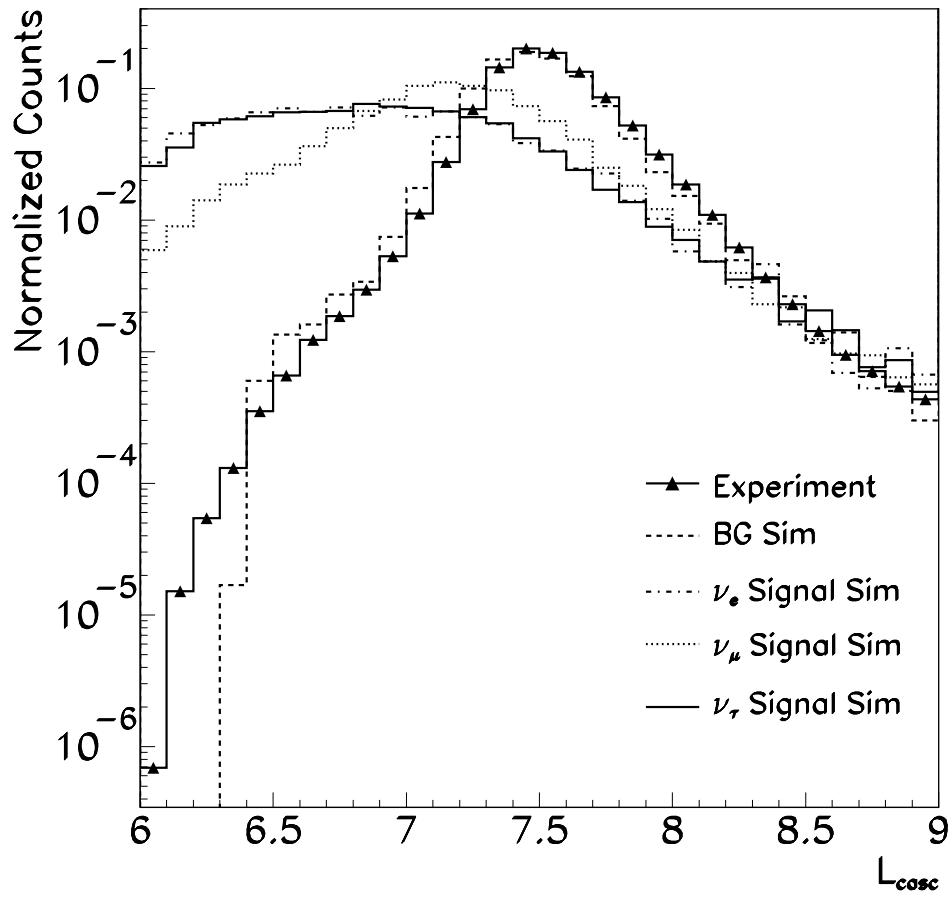


Fig. 7.— Distribution of L_{casc} for the experiment, background, and E^{-2} electron, muon, and tau neutrino signal simulations after level 2 of this analysis. Events with $L_{\text{casc}} < 7$ are “cascade-like,” and events with $L_{\text{casc}} \geq 7$ are “muon-like.”

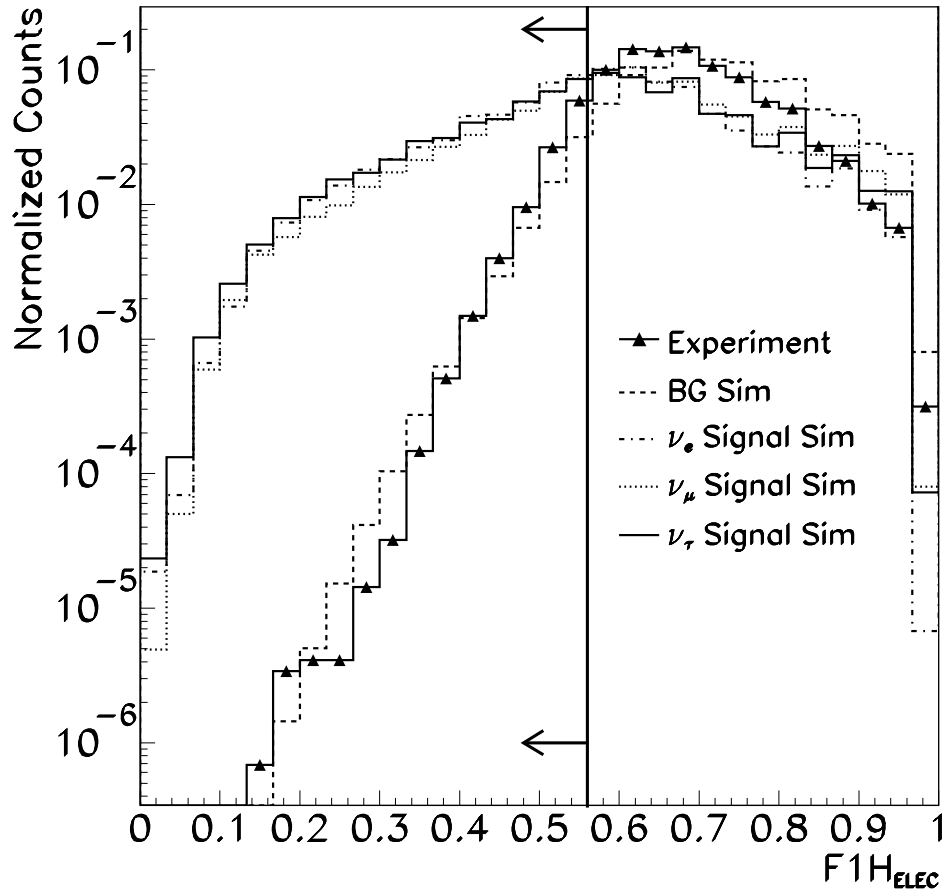


Fig. 8.— $F1H_{ELEC}$ (the fraction of electrical OMs with a single hit) distribution for the experiment, background, and E^{-2} electron, muon, and tau neutrino signal simulations in the “cascade-like” subset after level two of this analysis.

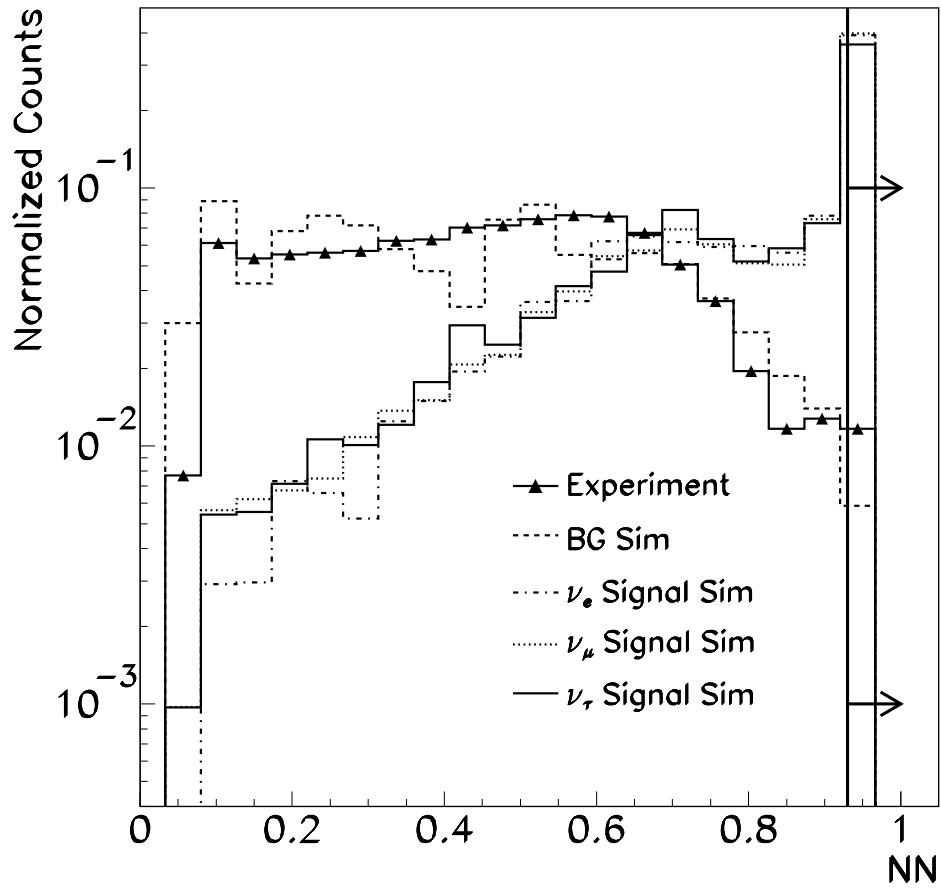


Fig. 9.— Distribution of neural net output for the experiment, background, and E^{-2} electron, muon, and tau neutrino signal simulations in the “cascade-like” subset after level two of this analysis. Signal events are expected near one, while background events are expected near zero.

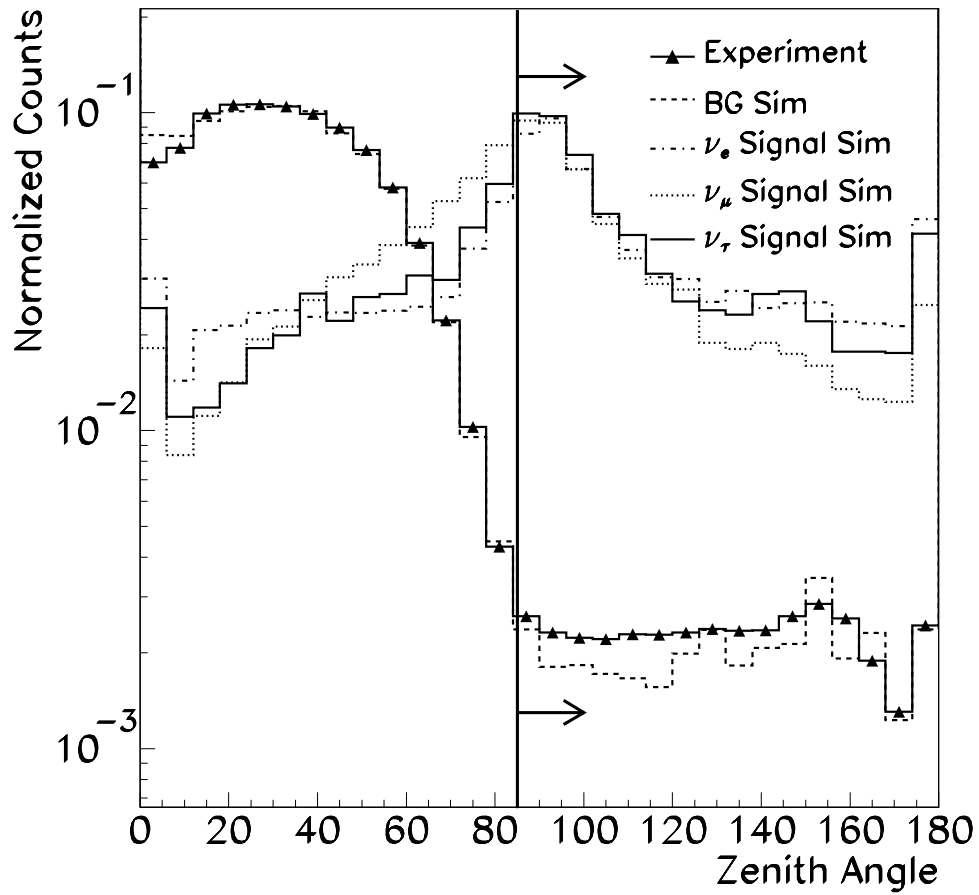


Fig. 10.— Reconstructed zenith angle distribution for the experiment, background, and E^{-2} electron, muon, and tau neutrino signal simulations in the “muon-like” subset after level two of this analysis. Zenith angles of 90° correspond to horizontal events, and zenith angles of 0° are downgoing events.

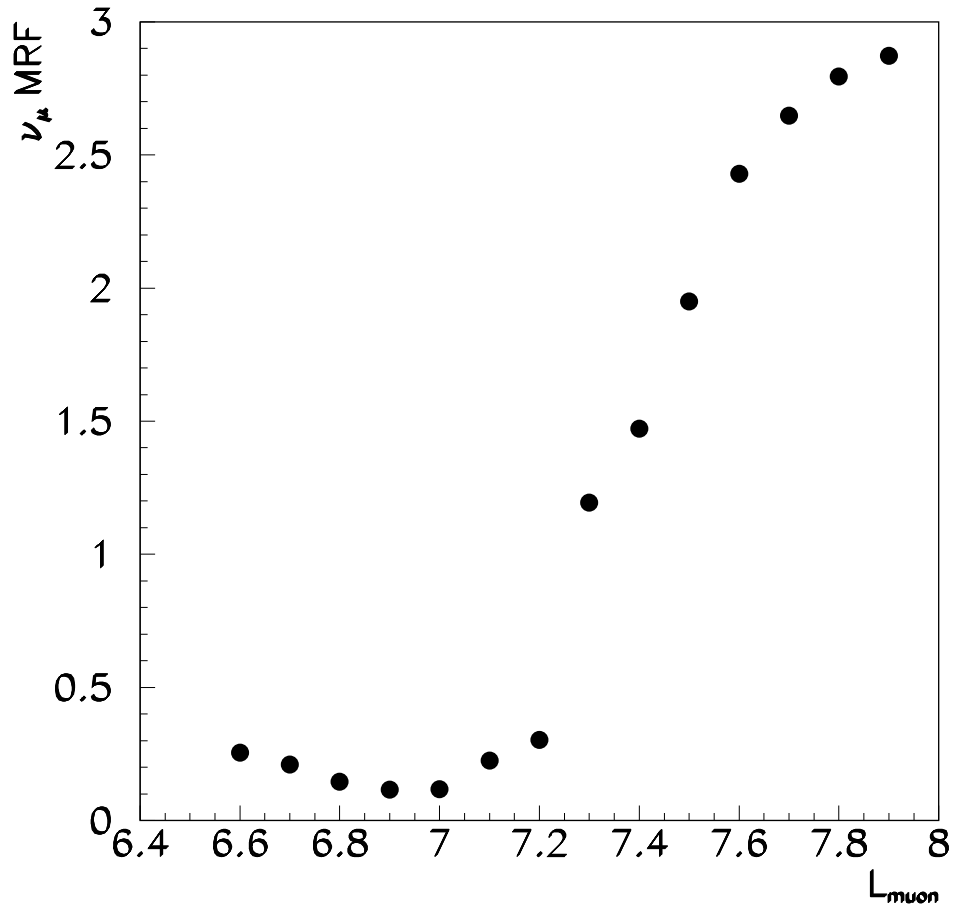


Fig. 11.— Model rejection factor for $10^{-6} \times E^{-2}$ muon neutrinos in the “muon-like” subset as a function of cut level for L_{muon} .

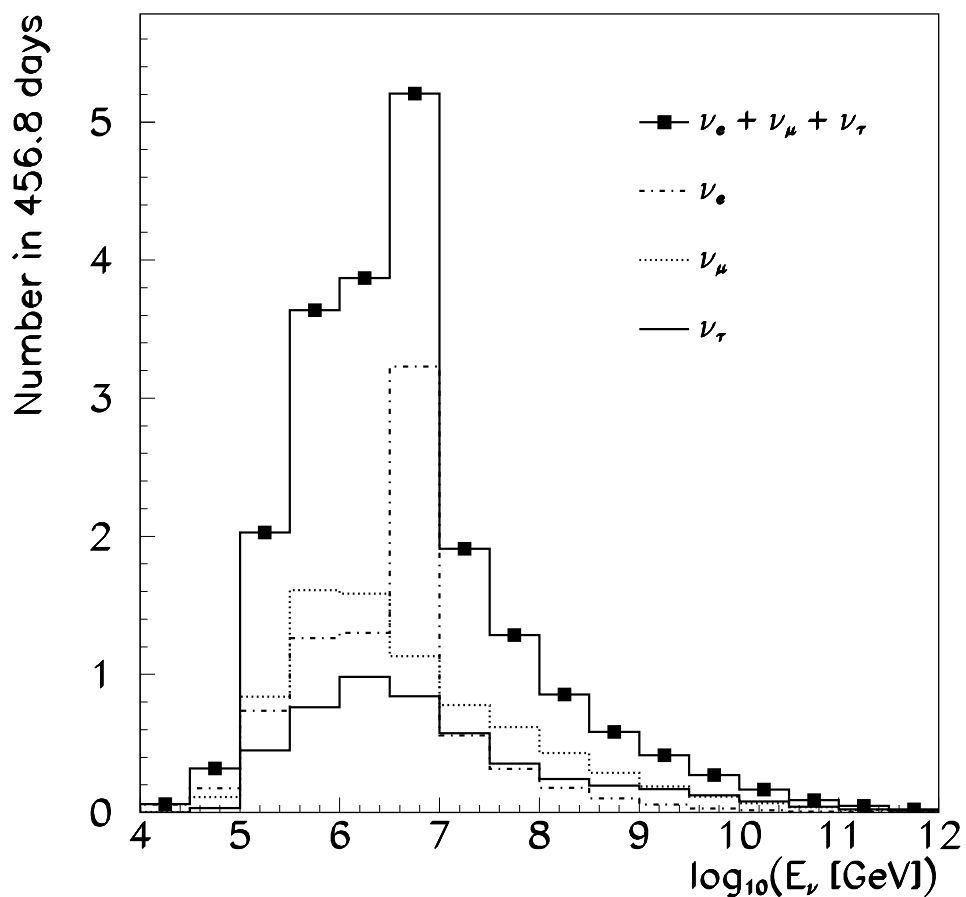


Fig. 12.— Energy spectra of electron, muon, and tau neutrino signal events ($d(N_{\nu_e}+N_{\nu_\mu}+N_{\nu_\tau})/dE = 10^{-6} \times E^{-2} \text{ GeV}^{-1} \text{ cm}^{-2} \text{ s}^{-1} \text{ sr}^{-1}$) which pass all selection criteria. The peak in the electron neutrino spectrum just below 10^7 GeV is due to the Glashow resonance.

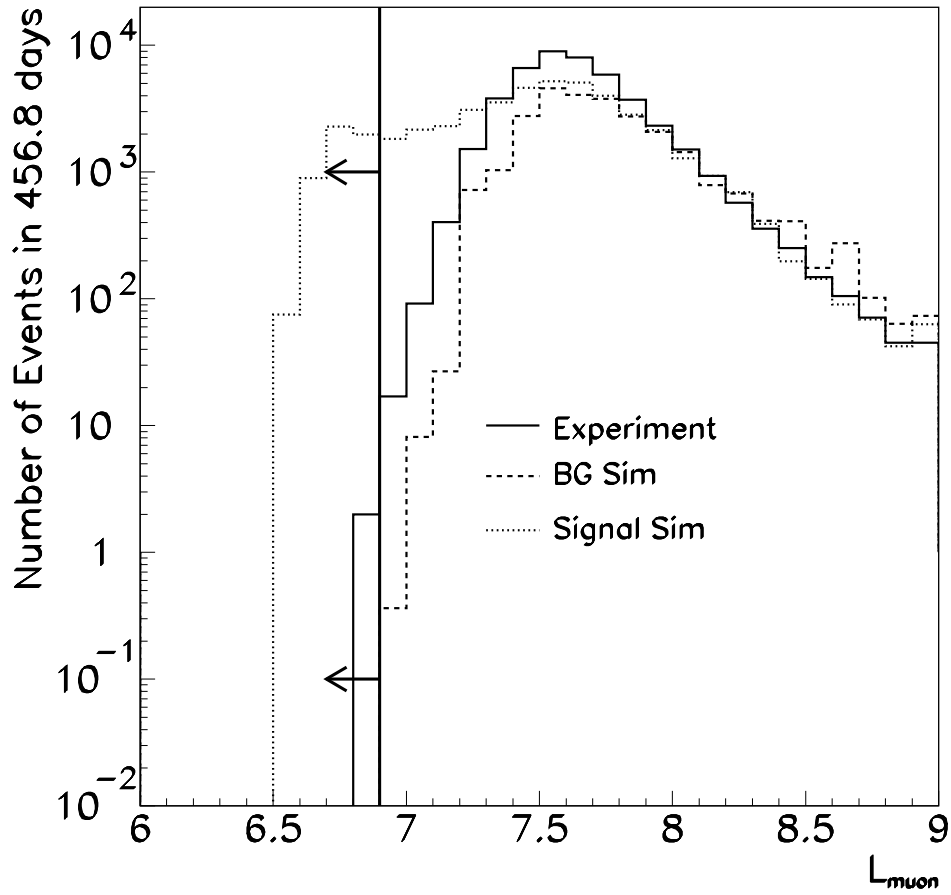


Fig. 13.— $L_{\mu\text{on}}$ distribution for the experiment, background, and $4.5 \times 10^{-4} \times E^{-2}$ muon neutrino signal simulations (arbitrary normalization) in the “muon-like” subset after level three of this analysis. Two experimental events survive the final selection criteria of $L_{\mu\text{on}} < 6.9$.

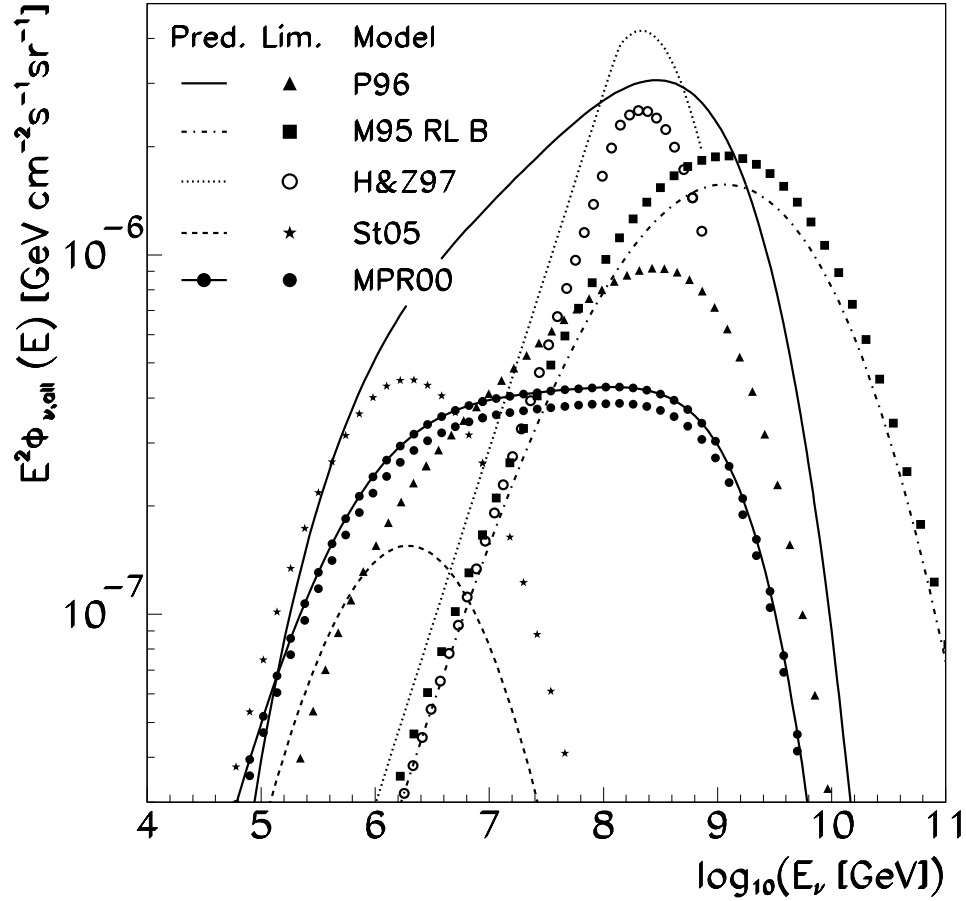


Fig. 14.— AGN fluxes tested in this paper. Lines denote the model predictions and symbols denote the 90% CL limits on the predictions derived by this analysis. The models rejected at the 90% CL shown are: H&Z97 from Halzen & Zas (1997), P96 from Protheroe (1996), and MPR00 from Mannheim et al. (2000). Also shown are models close to being rejected: M95 RL B from Mannheim (1995) and St05 from Stecker (2005). See Table 6 for exact numbers.

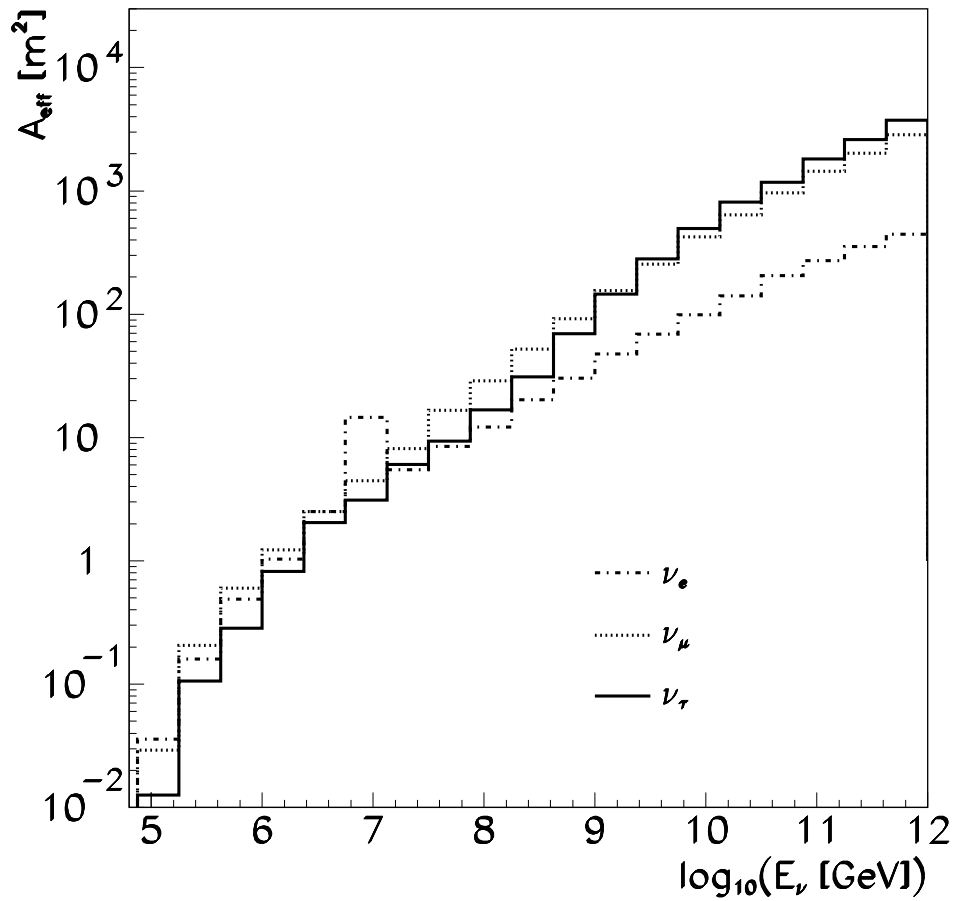


Fig. 15.— Angle-averaged neutrino effective area at final selection level as a function of neutrino energy for electron, muon, and tau neutrinos. The peak in the electron neutrino effective area just below 10^7 GeV is due to the Glashow resonance.